Pergamon

Geochimica et Cosmochimica Acta, Vol. 67, No. 1, pp. 123–131, 2003

0016-7037/03 $22.00 + .00

PII S0016-7037(02)01047-5

Temperature dependence of Pt and Rh solubilities in a haplobasaltic melt

S. S. FORTENFANT,[1] D. GÜNTHER,[2,*] D. B. DINGWELL,[3] and D. C. RUBIE[1]

[1]Bayerisches Geoinstitut, University of Bayreuth, D-95440 Bayreuth, Germany
[2]Laboratory for Inorganic Chemistry, Universitätsstr. 6, ETH Zürich, CH-8092 Zürich, Switzerland
[3]Department of Earth and Environmental Sciences, Theresienstr. 41, University of Munich, D-80333 Munich, Germany

(*Received July* 2, 2001; *accepted in revised form July* 2, 2002)

Abstract—The temperature dependence of the solubilities of Pt and Rh in a haplobasaltic (anorthite-diopside 1-bar eutectic composition) melt has been investigated at 1 bar and 1300 to 1550°C using the mechanically assisted equilibration technique (Dingwell et al., 1994). The experiments were performed at almost constant oxygen fugacity ($\log fO_2 = -2.5 \pm 0.3$) over the entire temperature range. Major element concentrations in the quenched glass samples were determined using an electron microprobe. Pt and Rh concentrations were obtained by laser ablation inductive coupled plasma mass spectrometry. From our data, we obtain the following expressions for the solubilities of pure Pt and pure Rh in anorthite-diopside eutectic melt at 1 bar and $\log fO_2 = -2.5$:

$$\log[\mathrm{Pt}](\mathrm{ppm}) = -\frac{3320(340)}{T(\mathrm{K})} + 2.0(0.2) \quad r^2 = 0.96,$$

$$\log[\mathrm{Rh}](\mathrm{ppm}) = -\frac{5440(450)}{T(\mathrm{K})} + 3.9(0.3) \quad r^2 = 0.97.$$

Metal-silicate partition coefficients estimated from these results at likely conditions of core formation (3000 K and an oxygen fugacity 2 orders of magnitude below the iron-wüstite oxygen buffer; e.g., Righter and Drake, 1997) are 6.1×10^8 and 3.9×10^6 for Pt and Rh, respectively. On the basis of these results, high temperature is not sufficient to explain the abundances of these highly siderophile elements in the Earth's mantle as a consequence of metal-silicate equilibrium during core formation.

1. INTRODUCTION

The overabundance of siderophile elements in the Earth's mantle remains an enigma for geochemists. Different models of Earth's accretion and core segregation have been proposed to explain the siderophile element anomaly (e.g., Jones and Drake, 1986; O'Neill, 1991; Li and Agee, 1996; Righter and Drake, 1997; Righter et al., 1997; Murthy and Karato, 1997; Walker, 2000). Such models can be divided into two groups that involve either heterogeneous accretion with multistage equilibrium between core and mantle or homogeneous accretion with high-pressure, high-temperature core-mantle equilibrium. Li and Agee (1996), for example, proposed that the core segregated from a magma ocean and that the abundance of siderophile elements can be explained by metal-silicate equilibrium at the base of the magma ocean (depth of ~750 km, pressure of ~28 GPa). This model explains successfully the abundances of the moderately siderophile elements Ni and Co in the mantle. However, it is doubtful if high-pressure equilibration models can explain the abundances of highly siderophile elements (HSEs) (Pt group elements, Re and Au) (e.g., Holzheid et al., 2000). In addition, although the ratios of the HSEs in the mantle are chondritic, their metal-silicate partition coefficients at 1 bar can differ by several orders of magnitude (O'Neill, 1991). Thus, to explain HSE abundances in the mantle by metal-silicate equilibrium, partition coefficients would need to have similar values and be orders of magnitude smaller than at 1 bar. The most successful model for explaining the abundances of the HSEs and their chondritic ratios involves the accretion of a late chondritic veneer after the core segregated from the mantle (e.g., Kimura et al., 1974; O'Neill, 1991).

To better constrain core formation models, knowledge of the effects of temperature, pressure, oxygen fugacity, and phase compositions on the solubilities of the HSEs in silicate melts is required to fully quantify their partitioning behaviour. Thus, for more than 10 years, the effects of different physicochemical parameters on HSE solubility in melts have been studied. Pt and Rh solubilities have been investigated as a function of fO_2 (Borisov and Palme, 1997; Ertel et al., 1999).

A recent study of Pd and Pt partitioning between metal and silicate melt suggests that pressure has little effect on the partitioning of these elements (Holzheid et al., 2000). The temperature dependences, vital for the extrapolation of results to the conditions of interest, are poorly known for Rh and have been studied for Pt by Borisov and Palme (1997) at three different oxygen fugacities. On the basis of experiments performed at 1 bar in pure O_2 using the conventional wire-loop method, Borisov and Palme (1997) showed that Pt solubility increases with increasing temperature. Solubility data obtained in air and pure CO_2 show a kink in the temperature dependence that is difficult to interpret. A difficulty in such studies is that metallic particles (micronuggets) can be present in the quenched silicate glasses and drastically contaminate the analyses. Solubility data obtained at low oxygen fugacities are

* Author to whom correspondence should be addressed (sophie.fortenfant@uni-bayreuth.de).

frequently affected by the presence of micronuggets (Borisov and Palme, 1997, 1998; Ertel et al., 1999, 2001). It is not clear whether the Pt solubility data of Borisov and Palme (1997) obtained in air and pure CO_2 were affected by micronuggets. However, it has been reported recently that Pt solubility data obtained using the same experimental technique at an oxygen fugacity of $10^{-3.1}$ bar (pure CO_2 atmosphere) showed serious contamination by micronuggets, whereas samples from experiments performed in air were relatively free of the problem (Ertel et al., 1999).

To clarify whether the temperature dependence of Pt solubility proposed by Borisov and Palme (1997) reflects a micronugget contamination problem, we have reexamined the effect of temperature on the solubility of Pt in silicate liquid through a study at 1 bar using the mechanically assisted equilibration technique. This technique, compared to the static "loop technique," is a dynamic technique that is believed to reduce the micronugget contamination problem (Ertel et al., 2001). Because our experiments were performed using Pt-Rh alloy, we have also obtained new results for the temperature dependence of Rh solubility in silicate melt. The new results are used to better constrain the behaviour of HSEs during core formation.

2. EXPERIMENTAL METHODS

To synthesize the starting material with the 1-bar anorthite-diopside eutectic composition, SiO_2, Al_2O_3, $MgCO_3$, and $CaCO_3$ powders were mixed in stoichiometric proportions, each oxide mass being corrected for volatility. The powder mixture was melted in an alumina crucible in air in a high-temperature box furnace at 1450°C. To quench the silicate, the crucible was removed from the oven and allowed to cool in air. After cooling, the crucible was broken, and glass chips free of alumina were separated for use in the experiments.

The mechanically assisted equilibration technique, described by Dingwell et al. (1994), has enabled solubility data for several HSEs, including Pt, Rh, Re, and Ni, to be obtained over wide ranges of temperature, fO_2, and composition (Ertel et al., 1996, 1999, 2001). A silicate melt contained in a crucible consisting of the metal or alloy of interest is stirred by a spindle fabricated from the same metal or alloy in a vertical, high-temperature furnace under a controlled atmosphere that determines the oxygen fugacity. For our study, the crucible and spindle were both made of a Pt-Rh alloy (80 wt.% Pt, 20 wt.% Rh).

The crucible, loaded with ~30 g of chips of silicate glass, was placed in the hot zone of a vertical, high-temperature furnace under oxygen fugacity conditions such that $\log fO_2 = -2.5$. The temperature was then raised to an initial value of 1300°C. Once the glass chips were molten, the spindle was introduced into the melt to stir it. To sample the silicate melt without stopping the experiment, the spindle was removed and the end of an alumina rod was slowly dipped into the melt. After removing the rod, the drop of melt hanging at its end was rapidly quenched in distilled water. The resulting glass sample of ~0.5 to 1 g was then dried and stored until analysis. After 10 days at 1300°C, the temperature was increased in steps of 50°C every 5 weeks to provide time for the melt to equilibrate at each temperature. An advantage of this technique is that large homogeneous glass samples are produced that can be easily analysed. Sampling at frequent time intervals enables the attainment of equilibrium to be monitored and the solubility of the elements of interest in the silicate melt to be determined for each temperature.

The oxygen fugacity (fO_2) was constrained by pure CO_2 gas flowing through the muffle tube of the furnace and was constantly monitored by means of an oxygen sensor placed directly below the crucible. The emf of the oxygen fugacity cell was constantly measured using a high-precision voltmeter permanently connected to the sensor. From the emf readings, we calculated oxygen fugacities between $10^{-2.5}$ and $10^{-2.1}$ bar. The highest fO_2 that can be provided by pure CO_2 is 10^{-3} bar (Nafziger et al., 1971). The discrepancy between this theoretical limit and the measured fO_2 values in our experiment is likely due to a leak in the furnace that allowed air to penetrate into the muffle tube, leading to experimental fO_2 conditions more oxidizing than planned. Importantly, the oxygen sensor used for the experiment was not defective. Indeed, its reliability was regularly checked during the experiment by changing the CO/CO_2 ratio of the gas each time the temperature was changed and measuring the corresponding emf. The results of such tests agreed well with the theoretical oxygen fugacities and confirmed the reliability of the sensor.

3. ANALYTICAL PROCEDURES

3.1. Major Elements

Major element (Si, Mg, Ca, and Al) concentrations in the glass samples were determined at the Bayerisches Geoinstitut using a Cameca SX-50 electron microprobe. The accelerating voltage was 20 kV, the beam current was 30 nA, and the counting time for each element was 20 s. The standards were orthoclase (Si), enstatite (Mg), wollastonite (Ca), and $MgAl_2O_4$ spinel (Al). For each sample, the major element contents were averaged from a linear profile of 20 points. Results show that all the samples are chemically homogeneous in major elements, as detailed in Table 1.

3.2. Trace Elements

The samples were analysed for Rh and Pt using laser ablation-inductively coupled plasma-mass spectrometry (LA-ICP-MS). A 193 Arf excimer laser (Lambda Physik, Göttingen, Germany) was coupled to an Elan 6100 DRC ICP mass spectrometer (Perkin Elmer, Norwalk, CT), which has been described elsewhere (Günther et al., 1997). The laser fluence was adjusted to 20 J/cm^2, and a crater diameter of 80 μm at a repetition rate of 10 Hz was used for the analysis. Helium admixed with argon was used as the carrier gas for the aerosol transport from the ablation cell to the ICP mass spectrometer. External calibration was carried out using in-house reference materials (Rh = 11.9 ppm, Pt = 4.01 ppm) and Mg was used as internal standard. Thirty-three samples were analysed as unknown samples (three replicates for each sample, 135 individual analyses, including standards). The glass reference standard 610 from the National Institute of Standards and Technology (NIST) was measured as unknown using the in-house external calibration standard, and the data determined for the NIST glass were within 12% of the Rh and Pt values reported by Sylvester and Eggins (1997). In addition to the NIST glass, in all samples, the major element concentrations (Si, Al, Ca) were determined by LA-ICP-MS using Mg as an internal standard. These concentrations agree within 10% with the data measured using electron probe microanalysis. The data acquisition and data reduction procedures for LA-ICP-MS described in Longerich et al. (1996) were applied.

4. RESULTS

Figure 1 shows the evolution of Pt and Rh solubilities in the anorthite-diopside melt with time and temperature. On the basis of the results of Ertel et al. (1999), it was assumed that after Pt and Rh solubilities equilibrated initially at 1300°C, 1 week of stirring was sufficient for their solubilities to reattain equilibrium after each temperature change. Therefore, sampling was performed 1 week after each temperature change and was continued at weekly intervals for a period of 1 month before

Table 1. Experimental conditions and sample compositions determined using electron microprobe for major elements and laser ablation-inductively coupled plasma-mass spectrometry for Pt and Rh. Pt and Rh concentrations in the glass samples reflect equilibrium with 80 wt.% Pt–20 wt.% Rh alloy.

				SiO_2		Al_2O_3		MgO		CaO		Pt ppm[a]				Rh ppm	
Sample	Time (h)	T (°C)	log fO_2	wt.%	SD	wt.%	SD	wt.%	SD	wt.%	SD	^{194}Pt[a]	SD	^{195}Pt[a]	SD	^{103}Rh[a]	SD
0	0	1300	–2.5	51.4	1.6	15.7	1.0	9.8	0.3	23.1	0.4	0.073	0.046	0.023	0.060	0.007	0.006
1	27	1300	–2.6	51.6	0.0	15.9	0.0	9.8	0.0	22.7	0.1	0.620	0.090	0.623	0.135	1.520	0.010
2	54	1300	–2.6	51.5	0.1	16.0	0.0	9.8	0.0	22.8	0.1	0.673	0.072	0.647	0.023	1.540	0.020
3	70	1300	–2.5	51.4	0.1	16.0	0.0	9.6	0.0	22.6	0.1	0.713	0.031	0.687	0.078	1.500	0.010
4	95	1300	–2.5	51.4	0.0	16.0	0.0	9.8	0.0	22.8	0.1	0.633	0.076	0.673	0.031	1.390	0.070
5	123	1300	–2.5	51.4	0.0	16.0	0.0	9.8	0.0	22.8	0.1	0.663	0.069	0.673	0.057	1.300	0.030
6	141	1300	–2.5	51.4	0.1	16.1	0.1	9.8	0.0	22.8	0.1	0.587	0.090	0.717	0.029	1.110	0.050
7	240	1300	–2.5	51.3	0.1	16.1	0.0	9.8	0.0	22.8	0.1	0.563	0.015	0.497	0.032	0.927	0.035
8	262	1350	–2.4	51.2	0.2	16.3	0.1	9.7	0.1	22.7	0.1	0.557	0.015	0.473	0.050	0.950	0.098
9	286	1350	–2.4	51.4	0.1	16.1	0.0	9.8	0.0	22.8	0.1	0.547	0.111	0.510	0.017	1.040	0.010
10	309	1350	–2.4	51.3	0.1	16.3	0.1	9.8	0.0	22.7	0.1	0.670	0.040	0.680	0.042	0.975	0.007
11	501	1350	–2.5	51.5	0.1	16.2	0.1	9.8	0.1	22.5	0.1	0.700	0.300	0.734	0.395	0.995	0.085
12	646	1350	–2.6	51.5	0.1	16.2	0.1	9.8	0.1	22.5	0.1	0.513	0.046	0.531	0.071	1.080	0.015
13	819	1350	–2.4	51.5	0.3	16.2	0.1	9.8	0.1	22.5	0.2	0.545	0.078	0.532	0.071	1.040	0.017
14	960	1350	–2.5	51.5	0.1	16.2	0.1	9.8	0.1	22.5	0.1	0.517	0.048	0.566	0.069	1.074	0.009
15	1179	1400	–2.5	51.5	0.1	16.2	0.1	9.8	0.1	22.5	0.1	0.589	0.053	0.617	0.042	1.280	0.024
16	1342	1400	–2.4	51.6	0.1	16.2	0.0	9.8	0.1	22.5	0.1	0.624	0.022	0.623	0.026	1.340	0.052
17	1509	1400	–2.4	51.4	0.1	16.2	0.1	9.8	0.1	22.5	0.1	0.678	0.129	0.631	0.079	1.200	0.005
18	1678	1400	–2.5	51.5	0.2	16.2	0.1	9.7	0.1	22.5	0.1	0.653	0.015	0.640	0.040	1.340	0.030
19	1848	1400	–2.4	51.6	0.2	16.2	0.1	9.8	0.1	22.5	0.1	0.727	0.081	0.750	0.020	1.500	0.010
20	2014	1450	–2.5	51.5	0.2	16.3	0.1	9.7	0.1	22.4	0.1	0.723	0.149	0.773	0.071	1.670	0.110
21	2183	1450	–2.4	51.7	0.2	16.3	0.1	9.7	0.1	22.3	0.1	0.917	0.154	0.793	0.068	1.860	0.030
22	2374	1450	–2.4	51.6	0.2	16.3	0.1	9.7	0.1	22.4	0.1	0.860	0.295	0.723	0.055	1.760	0.130
23	2523	1450	–2.4	51.3	0.1	16.4	0.0	9.7	0.0	22.6	0.1	0.840	0.010	0.770	0.078	1.910	0.020
24	2614	1450	–2.4	51.3	0.1	16.3	0.0	9.7	0.0	22.7	0.1	0.963	0.071	0.887	0.133	1.910	0.040
25	2614	1450	–2.4	51.3	0.1	16.3	0.0	9.8	0.0	22.7	0.1	0.863	0.038	0.890	0.026	1.990	0.040
26	2971	1450	–2.4	51.3	0.1	16.3	0.1	9.7	0.1	22.6	0.1	0.803	0.060	0.903	0.075	1.820	0.030
27	3162	1500	–2.1	51.3	0.1	16.3	0.1	9.7	0.1	22.6	0.1	1.000	0.060	1.000	0.080	2.390	0.010
28	3307	1500	–2.1	51.3	0.1	16.3	0.1	9.7	0.1	22.6	0.1	1.130	0.020	1.210	0.060	2.290	0.100
29	3476	1500	–2.1	51.3	0.1	16.3	0.1	9.7	0.1	22.6	0.1	1.060	0.040	1.060	0.060	2.280	0.100
30	3643	1500	–2.1	51.3	0.1	16.3	0.1	9.7	0.1	22.6	0.1	1.140	0.120	1.170	0.040	2.490	0.010
31	3814	1500	–2.1	51.3	0.1	16.3	0.1	9.7	0.1	22.6	0.1	1.050	0.120	1.000	0.040	2.390	0.020
32	4004	1500	–2.1	51.3	0.1	16.3	0.1	9.7	0.1	22.6	0.1	1.180	0.080	1.220	0.220	2.880	0.050

[a] Isotope used for detection on the mass spectrometer and to calculate total element concentration.

changing the temperature again. At 1550°C, the experiment had to be stopped because of the failure of a heating element, and sampling was performed only once at this temperature after 1 week of stirring, which should be sufficient time for equilibration.

As discussed above, solubility data from our experiments were obtained at oxygen fugacities ranging from log $fO_2 = -2.5$ to -2.1. The solubility data were recalculated to an oxygen fugacity of $10^{-2.5}$ bar using the following equation:

$$\log[M]_{\log fO_2=-2.5} = \log[M]_{\log fO_2} - 0.5 \times (\log fO_2 + 2.5), \quad (1)$$

where M represents Pt or Rh. For the purpose of this calculation, we assumed that Pt and Rh are present in the melt as +2 species. Because the experiment was performed over a narrow range of oxygen fugacities ($10^{-2.5}$ to $10^{-2.1}$ bar), the potential error introduced by this assumption is small. From the recalculated solubilities, equilibrium solubilities were estimated by averaging the concentrations determined over the 1-month sampling periods. In the case of Rh, the solubilities were determined from concentrations of the ^{103}Rh isotope and for Pt from concentrations of ^{194}Pt and ^{195}Pt. These averaged solubilities for Pt and Rh correspond to equilibrium between anorthite-diopside eutectic melt and 80 wt.% Pt–20 wt.% Rh alloy.

The solubilities of pure Pt and Rh in the melt can be deduced from the experimental solubilities using the following relationship:

$$[M](\text{ppm}) = \frac{[M]_{\text{exp}}(\text{ppm})}{X_M^{\text{met}} \times \gamma_M^{\text{met}}}, \quad (2)$$

where M is either Pt or Rh, $[M]$ is the solubility in the melt corresponding to equilibrium with pure metal, $[M]_{\text{exp}}$ is the measured solubility corresponding to equilibrium with the alloy, X_M^{met} is the mole fraction of M in the alloy, and γ_M^{met} is the activity coefficient of M in the alloy. The activity coefficients of Pt and Rh in the alloy can be estimated using mixing properties of the Pt-Rh binary system reported by Jacob et al. (1998). The excess Gibbs energy of mixing of the Pt-Rh binary alloy (in kJ/mol) is related to the mole fraction of Rh in the alloy according to the following equation:

$$\Delta_{\text{mix}}G^{\text{ex}}_{\text{Pt–Rh}} = X^{\text{met}}_{\text{Rh}}(1-X^{\text{met}}_{\text{Rh}})[(-10.970 + 0.0038 \times T) + (0.045 - 1.55 \times 10^{-5} \times T) \times X^{\text{met}}_{\text{Rh}}], \quad (3)$$

where T is temperature (in K). In a binary system A-B, the activity coefficients of A and B in the alloy, γ_A^{met} and γ_B^{met}

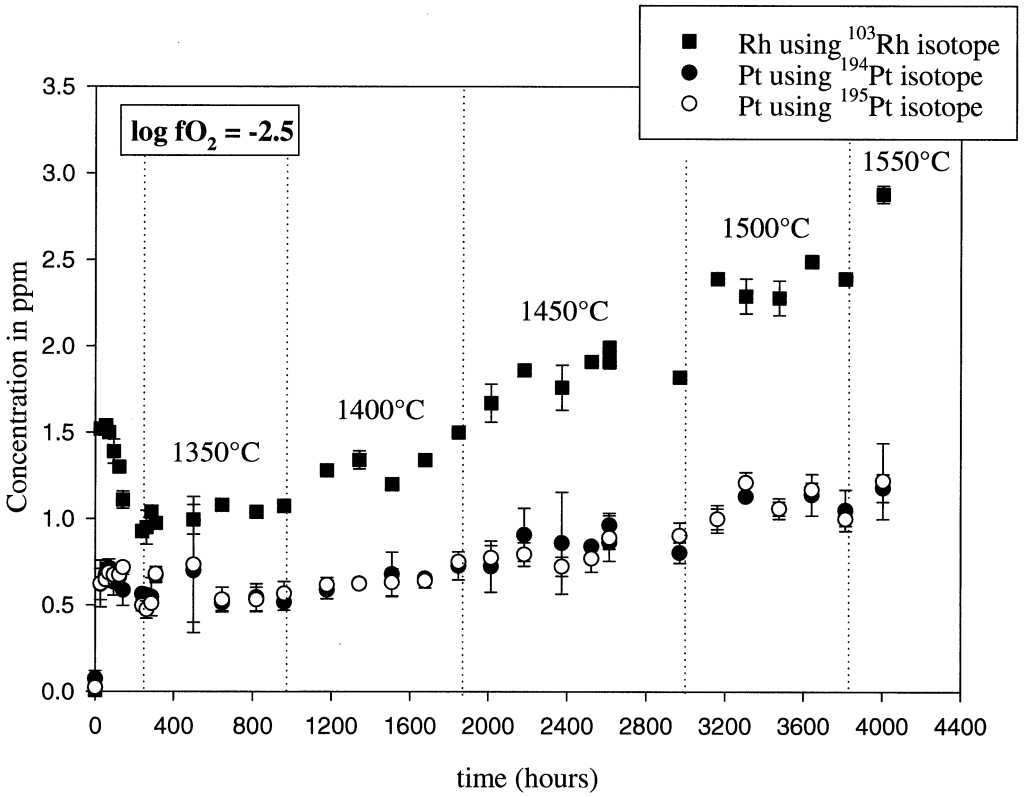

Fig. 1. Concentrations of Pt and Rh in quench glasses from time-series equilibration experiments on an anorthite-diopside eutectic melt in the temperature range 1300 to 1550°C at 1 bar pressure and oxygen fugacities in the range log $fO_2 = -2.5$ to -2.1. The analyses were performed using laser ablation-inductively coupled plasma-mass spectrometry. Concentrations reflect equilibrium with 80 wt.% Pt–20 wt.% Rh alloy.

respectively, are related to the excess Gibbs energy of mixing, $\Delta_{mix}G^{ex}$, according to the following equations:

$$RT\ln\gamma_A^{met} = \Delta_{mix}G^{ex} + (1-X_A)\frac{\partial\Delta_{mix}G^{ex}}{\partial X_A}, \quad (4)$$

$$RT\ln\gamma_B^{met} = \Delta_{mix}G^{ex} - X_A\frac{\partial\Delta_{mix}G^{ex}}{\partial X_A}, \quad (5)$$

where R is the gas constant, and X_A is the mole fraction of A in the binary alloy A-B. If the Redlich-Kister formulation is adopted, the excess Gibbs energy of mixing can be written as (asymmetric regular solution) follows:

$$\Delta G_{A-B}^{ex} = X_A(1-X_A)(a_0 + a_1(1-2X_A) + a_2(1-2X_A)^2 + \cdots), \quad (6)$$

where a_0, a_1, a_2, and so on are constants that are independent of X_A but may be temperature and pressure dependent. Eqn. 4 and 5 become

$$RT\ln\gamma_A^{met} = (1-X_A)^2(a_0 + a_1(1-4X_A) + a_2(1-2X_A)(1-6X_A) + \cdots), \quad (7)$$

$$RT\ln\gamma_B^{met} = X_A^2(a_0 + a_1(3-4X_A) + a_2(1-2X_A)(5-6X_A) + \cdots). \quad (8)$$

Using Eqn. 3, 7, and 8, we calculated the activity coefficients of Pt and Rh in the 80 wt.% Pt–20 wt.% Rh alloy for each experimental temperature. These activity coefficients, as well as the solubilities of pure Pt and Rh in haplobasaltic melt at log $fO_2 = -2.5$, calculated using Eqn. 2, are listed as a function of temperature in Table 2.

The solubilities of pure Pt and Rh in haplobasaltic melt at log $fO_2 = -2.5$ are plotted against inverse temperature in Figure 2. For both elements, the solubility in the melt increases with increasing temperature. Fits of the data for Pt and Rh give the following expressions for the solubilities of pure Pt and pure Rh in haplobasaltic melt as a function of temperature at:

$$\log[\text{Pt}](\text{ppm}) = -\frac{3320(340)}{T(\text{K})} + 2.0(0.2) \quad r^2 = 0.96, \quad (9)$$

$$\log[\text{Rh}](\text{ppm}) = -\frac{5440(450)}{T(\text{K})} + 3.9(0.3) \quad r^2 = 0.97. \quad (10)$$

5. DISCUSSION

5.1. Effects of Temperature and Oxygen Fugacity on the Solubilities of Pt and Rh

Borisov and Palme (1997) determined the solubility of Pt in silicate melt up to 1550°C over an oxygen fugacity range from log $fO_2 = -8$ to pure oxygen. A plot of Pt solubility against oxygen fugacity gave a slope of 0.5, suggesting a valence of $+2$ for Pt in the melt. At oxygen fugacities $<10^{-5}$ bar, an

Table 2. Temperature dependence of Pt and Rh solubilities in anorthite-diopside melt at 1 bar and log fO_2 = –2.5

	Equilibrium with $Pt_{0.68}Rh_{0.32}$ alloy						Equilibrium with pure metal			
T (°C)	[Rh] (ppm)	SD	[Pt] (ppm)[a]	SD	log γ_{Rh}^{metb}	log γ_{Pt}^{metb}	[Rh] (ppm)	SD	[Pt] (ppm)[a]	SD
1300	0.945	—	0.548	—	0.952	1.069	3.101	—	0.754	—
1350	1.020	0.068	0.573	0.216	0.955	1.065	3.337	0.223	0.792	0.299
1400	1.314	0.113	0.635	0.094	0.958	1.060	4.286	0.367	0.881	0.130
1450	1.837	0.076	0.813	0.108	0.961	1.056	5.974	0.248	1.132	0.151
1500	2.155	0.086	0.895	0.125	0.964	1.052	6.986	0.278	1.251	0.175
1550	2.669	—	0.989	—	0.966	1.048	8.632	—	1.388	—

[a] Average from both Pt estimates on the basis of ^{194}Pt and ^{195}Pt isotope concentrations, respectively.
[b] Activity coefficients estimated using thermodynamic data of Jacob et al. (1998).

apparent increase in the Pt solubility was observed and attributed to the presence of micronuggets that would have formed in the melt because of the reducing atmosphere. Recently, Ertel et al. (1999) reported Pt and Rh solubilities in haplobasaltic melt using the same technique as used in the present study. With LA-ICP-MS microanalysis techniques, Ertel et al. (1999) were able to avoid micronugget contamination in sample analysis. Ertel et al. (1999) suggested the presence of Pt^{2+} and Rh^{2+} with evidence of Pt^{4+} and Rh^{3+} at the highest oxygen fugacities studied (air and pure O_2). The solubility data of Ertel et al. (1999) were calculated assuming ideal behaviour of Pt and Rh in the 80 wt.% Pt–20 wt.% Rh alloy used for the experiment. The data of Jacob et al. (1998) were not available at the time Ertel et al. (1999) submitted their paper.

At 1300°C, the activity coefficients of Pt and Rh in the alloy are 0.95 and 1.07, respectively. By using these activity coefficients to correct the solubility equations for Pt and Rh of Ertel et al. (1999), the solubilities of Pt and Rh as a function of oxygen fugacity at 1300°C are given by the following equations:

$$[\text{Pt}](\text{ppb}) = 1960(fO_2) + 10{,}260(fO_2)^{1/2}, \quad (11)$$

$$[\text{Rh}](\text{ppb}) = 72{,}240(fO_2)^{3/4} + 33{,}120(fO_2)^{1/2}. \quad (12)$$

At 1300°C and log $fO_2 = -2.5$, the solubilities of Pt and Rh calculated using Eqn. 11 and 12 are 0.58 and 2.82 ppm, respectively. On the basis of on the coefficients in these equations, the Pt^{4+}/Pt^{2+} and Rh^{3+}/Rh^{2+} ratios are ~1.1 and 50%, respectively. In the present study, the solubilities of pure Pt and pure Rh at 1300°C and log $fO_2 = -2.5$ estimated using the fit

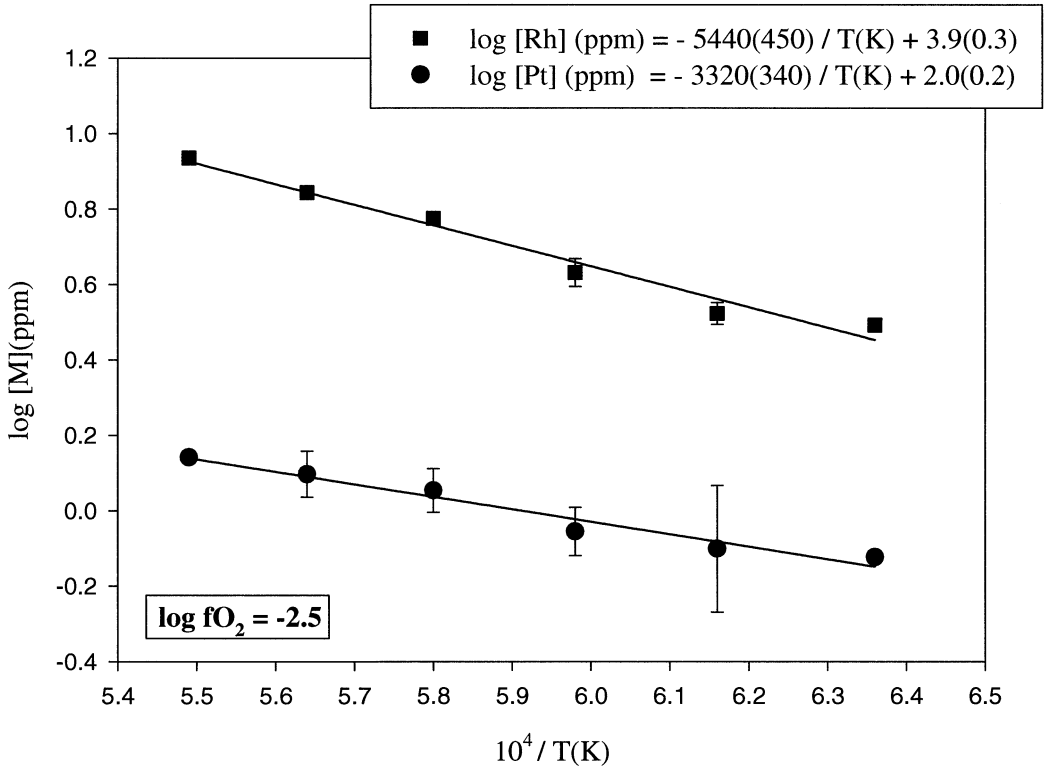

Fig. 2. Solubilities of pure Pt and Rh in an anorthite-diopside eutectic melt at 1 bar, log $fO_2 = -2.5$ and 1300 to 1550°C as a function of inverse temperature.

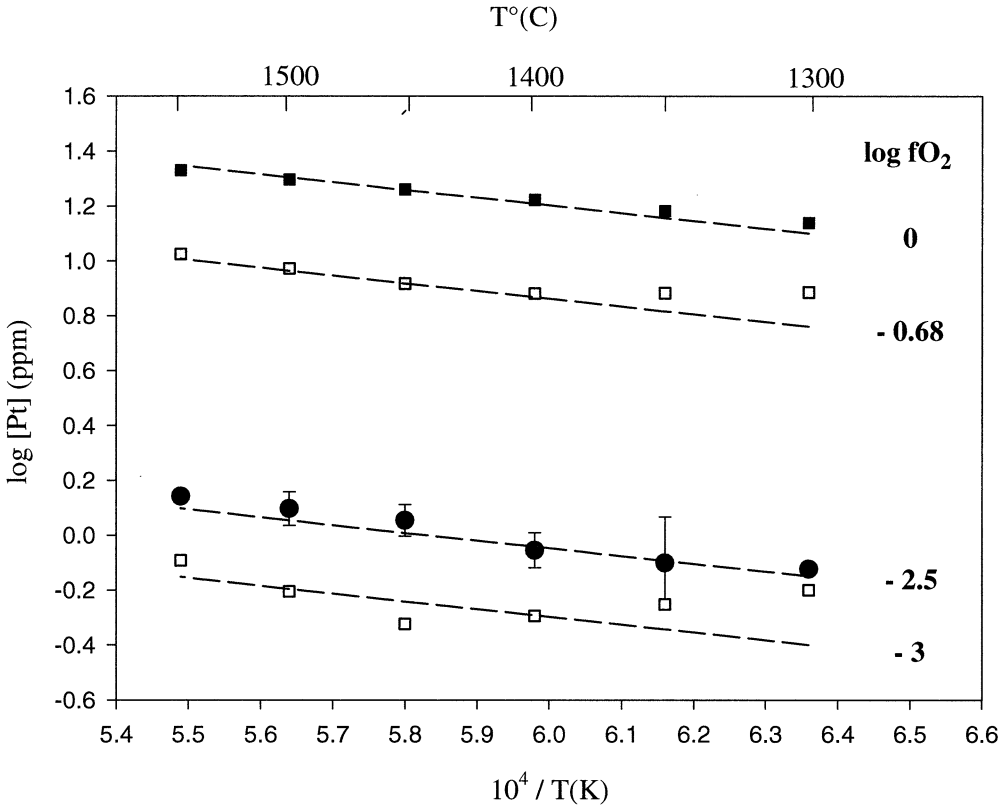

Fig. 3. Temperature dependences of Pt solubility in anorthite-diopside eutectic melt at 1 bar and at various fO_2 values from results of the present study (filled circles) and from Borisov and Palme (1997) (squares). The results of Borisov and Palme (1997) obtained in air and pure CO_2 atmospheres show a kink in the plots of solubility against inverse temperature (indicated by arrows on the graph). Such a kink is not observed in the present study. Broken lines show a linear fit of Eqn. 14 to the data as a function of temperature and oxygen fugacity.

Eqn. 9 and 10 are 0.72 and 2.75 ppm, respectively. These values are in good agreement with the values of Ertel et al. (1999) if we consider the uncertainties on the Pt and Rh solubilities from Ertel et al's (1999) equations (~10% for Pt and ~5% for Rh) and the uncertainties in oxygen fugacity in our experiment (±0.05 log units).

Borisov and Palme (1997) also gave the solubility of Pt in haplobasaltic melt as a function of temperature at 1 bar and for various oxygen fugacities (in pure O_2, in air, and in pure CO_2). The solubility of pure Pt as a function of temperature from our study are compared with the data of Borisov and Palme (1997) in Fig. 3. Over the upper part of the temperature range studied, the results of the two studies are in reasonable agreement. At lower temperatures (<1450°C), the results of Borisov and Palme (1997) obtained in air and pure CO_2 atmospheres show a kink in the plots of solubility against inverse temperature (Fig. 3). Such a kink in the low-temperature solubility trend is not observed in the present study. Possible causes of the relatively high solubilities observed by Borisov and Palme (1997) at low temperatures (1300 to 1450°C) and low fO_2 could be a contamination of the glass samples by micronuggets and/or a lack of equilibrium in their experiments. In the present study, the use of the stirred crucible method has apparently allowed us to produce solubility results for Pt and Rh free of such problems. Moreover, the time-series sampling allowed us to check for the equilibrium solubilities of both elements in the melt. We conclude therefore that over the oxygen fugacity range of Borisov and Palme's (1997) experiments and our study (from pure O_2 to 10^{-3} bar), the solubility of Pt in anorthite-diopside eutectic melt increases with increasing temperature.

The solubility of Pt in silicate melt as a function of temperature and oxygen fugacity can be estimated from Eqn. 9 if we assume that the valence of Pt in the silicate liquid is +2 (Pt^{4+}/Pt^{2+} ratio being ~ 1% at 1300°C, the effect of the contribution of Pt^{4+} species is neglected here). In this case

$$\log[\mathrm{Pt}](\mathrm{ppm}) = -\frac{3320(340)}{T(\mathrm{K})} + 2.0(0.2) + 0.5 \times (2.5 + \log fO_2). \quad (13)$$

Alternatively, the dependence can be determined by fitting our data together with the high-temperature (>1450°C) results of Borisov and Palme (1997) (assuming that their low-temperature data are affected by micronuggets, as discussed above). Such a fit gives the following expression:

$$\log[\mathrm{Pt}](\mathrm{ppm}) = -\frac{2830(290)}{T(\mathrm{K})} + 2.9(0.2) + 0.5(0.01) \times \log fO_2 \quad r^2 = 0.99, \quad (14)$$

which is consistent with a valence of +2.00(±0.04) for Pt.

Unlike Pt, for which Pt^{2+} remains predominant in silicate

melt over the whole temperature and oxygen fugacity range, in the case of Rh, Rh^{2+} and Rh^{3+} species are both present in melt in relatively high proportions (Ertel et al., 1999). It was calculated above that the ratio Rh^{3+}/Rh^{2+} is 50% at log $fO_2 = -2.5$ and 1300°C. Using the oxygen fugacity–solubility relationship of Ertel et al. (1999), the Rh^{3+}/Rh^{2+} ratio is predicted to decrease with decreasing oxygen fugacity. This ratio becomes ~1% at 1300°C and an oxygen fugacity of $10^{-9.35}$ bar. Thus, over the oxygen fugacity range of interest, Rh^{2+} is the predominant species. Because the redox equilibria always tend to the reduced state with increasing temperature at constant fO_2, it is therefore likely that the Rh^{3+}/Rh^{2+} ratio also decreases with increasing temperature (Prof. H. D. Schreiber, personal communication, 2001). In the present study, the Rh^{2+} species may therefore have become predominant in the melt as the temperature of the experiment was increased. Although Rh^{3+} might not be negligible relative to Rh^{2+} over the whole temperature range, it is assumed here, for convenience, that Rh dissolves in the melt predominantly as +2 species. Incorporating the term related to the oxygen fugacity effect into Eqn. 10 gives the following equation:

$$\log[\mathrm{Rh}](\mathrm{ppm}) = -\frac{5440(450)}{T(\mathrm{K})} + 3.9(0.3) + 0.5 \times (2.5 + \log fO_2). \quad (15)$$

5.2. Implications for Metal-Silicate Distribution Coefficients

The solubility equations presented above can be used to estimate the partitioning of Pt and Rh between metal and silicate liquid in a magma ocean during core formation (e.g., Li and Agee, 1996; Righter et al., 1997). This requires extrapolating the solubility results to the appropriate P, T, and fO_2 conditions and using them to estimate metal-silicate partition coefficients. Temperature and oxygen fugacity conditions in the magma ocean were likely ~2500 to 3000 K, with an oxygen fugacity ~2 log units below the iron-wüstite (IW) buffer, corresponding to an absolute oxygen fugacity of $10^{-4.2}$ bar at 3000 K (calculated by using the μ_{O_2}-T equation for the system Fe-FeO of O'Neill and Pownceby, 1993 and by correcting for the melting of Fe using the thermodynamic data of Swartzendruber, 1984).

At 3000 K and log $fO_2 = -4.2$ the solubility of Pt in anorthite-diopside liquid calculated using Eqn. 13 is 1.10 ± 0.09 ppm, and using Eqn. 14, it is 0.72 ± 0.07 ppm. The solubility of Rh at the same conditions estimated using Eqn. 15 is 17.2 ± 1.3 ppm.

Distribution coefficients for siderophile elements partitioning between Fe-rich metal and silicate melt, $D_M^{\mathrm{met/sil}}$, can be deduced from their solubilities in silicate melt at high temperature from the following equation:

$$D_M^{\mathrm{met/sil}} = \frac{1}{[M] \times \gamma_M^{\mathrm{Fe},\infty} \times A} \quad (16)$$

where $[M]$ is the solubility of M in silicate melt as weight fraction, $\gamma_M^{\mathrm{Fe},\infty}$ is the activity coefficient of M at infinite dilution in liquid iron referred to a standard state of pure solid metal M, and A is a factor to convert from mole fractions to weight fractions (Borisov et al., 1994). A is 0.29 for Pt and 0.54 for Rh. The activity coefficients of Rh in liquid iron referred to solid standard state can be estimated using the thermodynamic data for the binary system Fe-Rh of Swartzendruber (1984) and the following relationship:

$$RT\ln\gamma_M^{\mathrm{met}} = RT\ln\gamma_{M,\mathrm{liquid\ std\ state}}^{\mathrm{met}} + \Delta_{\mathrm{melt}}G_M, \quad (17)$$

where $\Delta_{\mathrm{melt}}G_M$ is the free energy of melting of M under standard conditions, and $\gamma_{M,\mathrm{liquid\ std\ state}}^{\mathrm{met}}$ is the activity coefficient of M in liquid iron referred to a standard state of liquid M. The activity coefficient of Rh in liquid iron referred to a standard state of liquid Rh can be estimated as described in the previous section using the equations for the excess Gibbs energies of mixing of liquid Fe-Rh of Swartzendruber (1984)):

$$\Delta_{\mathrm{mix}}G_{\mathrm{Fe-Rh}}^{\mathrm{ex}} = -10.883X_{\mathrm{Rh}}(1-X_{\mathrm{Rh}}), \quad (\mathrm{in\ kJ/mol}), \quad (18)$$

where X_{Rh} is the molar fraction of Rh in the Fe-Rh alloy. The free energy of melting of Rh is

$$\Delta_{\mathrm{melt}}G_{\mathrm{Rh}} = G_{\mathrm{Rh}}^{\circ}(\mathrm{liq}) - G_{\mathrm{Rh}}^{\circ}(\mathrm{fcc}) = 5.907 + 0.08233T - 0.01162T\ln T + 2.08 \times 10^{-6}T^2 \quad (\mathrm{in\ kJ/mol}). \quad (19)$$

With Eqn. 6, 7, 17, 18 and 19, the activity coefficient of Rh in liquid iron referred to a standard state of pure solid Rh can be calculated according to the following equation:

$$RT\ln\gamma_{\mathrm{Rh}}^{\mathrm{Fe},\infty} = -53.153 + 0.08233T - 0.01162T\ln T + 2.08 \times 10^{-6}T^2 \quad (\mathrm{in\ kJ/mol}). \quad (20)$$

To estimate the activity coefficient of Pt in liquid iron, we used the tabulated thermodynamic data for Fe-Pt liquid alloy binary of Hultgren et al. (1971). Data were fitted to find the appropriate interaction parameters, applying the formulism of asymmetric regular solution (Mukhopadhyay et al., 1993). From these data, the fit of the excess Gibbs energy of mixing of Fe-Pt liquid alloy as a function of the molar fraction of Pt, X_{Pt}, gives

$$\Delta_{\mathrm{mix}}G_{\mathrm{Fe-Pt}}^{\mathrm{ex}} = X_{\mathrm{Pt}}(1-X_{\mathrm{Pt}})[-117.34\ (\pm 3.79) + 38.96(\pm 1.26) \times (1-2X_{\mathrm{Pt}})]\ (\mathrm{in\ kJ/mol}) \quad (21)$$

Using the thermodynamic data for pure Pt of Barin (1989), the free energy of melting of Pt can be expressed as a function of temperature as follows:

$$\Delta_{\mathrm{melt}}G_{\mathrm{Pt}} = 9.47 + 0.069T - 0.0104T\ln T \quad (\mathrm{in\ kJ/mol}). \quad (22)$$

Again, according to Eqn. 6, 7, 21, and 22, the activity coefficient of Pt in liquid iron referred to a standard state of pure solid Pt can be calculated according to the following equation:

$$RT\ln\gamma_{\mathrm{Pt}}^{\mathrm{Fe\ liq},\infty} = -68.91 + 0.069T - 0.0104T\ln T\ (\mathrm{in\ kJ/mol}). \quad (23)$$

Using Eqn. 20 and 23, the activity coefficients of Pt and Rh at infinite dilution in liquid iron ($X_{\mathrm{Pt}} \to 0$ and $X_{\mathrm{Rh}} \to 0$), $\gamma_{\mathrm{Pt}}^{\mathrm{Fe},\infty}$ and $\gamma_{\mathrm{Rh}}^{\mathrm{Fe},\infty}$, are estimated to be 0.011 and 0.0695, respectively, at 3000 K. Note that these values are significantly higher than the activity coefficient values used by Ertel et al. (1999), which

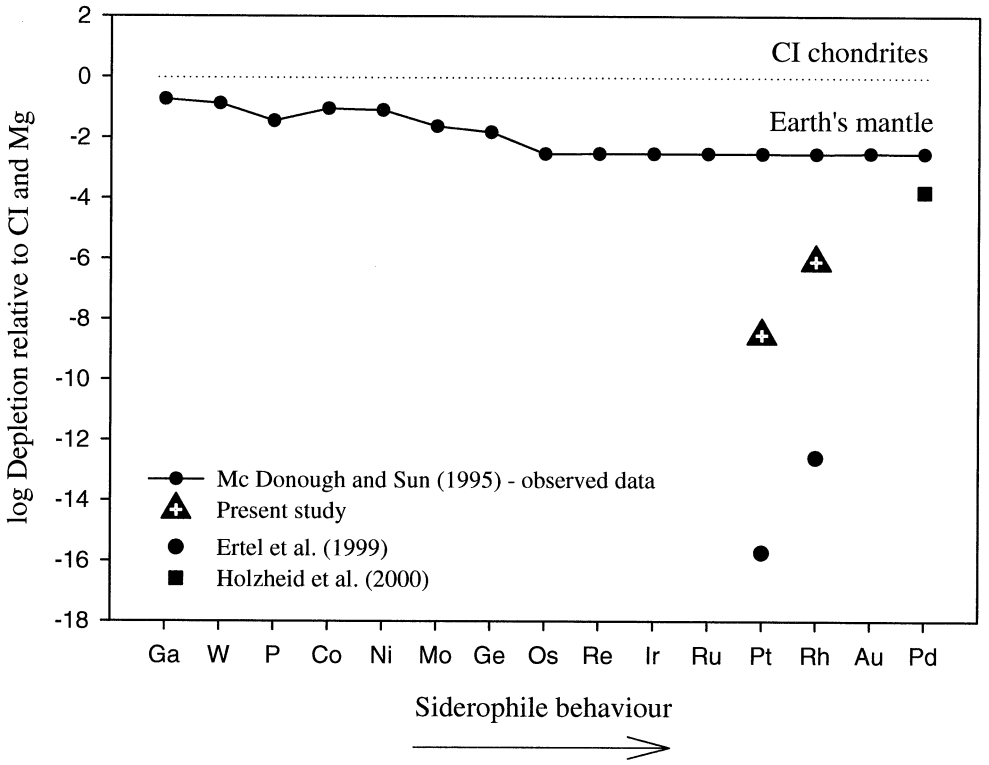

Fig. 4. Diagram showing the depletion of siderophile elements relative to CI chondrites and Mg. Observed depletion values for the mantle are calculated using estimated mantle abundances of the elements from McDonough and Sun (1995). Depletions of Pt, Rh, and Pd calculated assuming metal-silicate equilibration and using the values of metal-silicate melt partition coefficients of Pt, Rh, and Pd from the present study, from Ertel et al. (1999), and from Holzheid et al. (2000) are shown. High temperature remains insufficient to explain the observed abundances of Pt and Rh in the upper mantle, although it increases the predicted abundances significantly.

corresponded to infinite dilution in solid iron at 1573°C ($\gamma_{Pt}^{solid\ Fe,\infty} = 3 \times 10^{-5}$ and $\gamma_{Rh}^{solid\ Fe,\infty} = 1.5 \times 10^{-2}$). Using activity coefficient values of 0.011 and 0.00695 for Pt and Rh, respectively, and extrapolated solubility values of 0.72 ± 0.07 ppm for Pt and 17.2 ± 1.3 ppm for Rh at 3000 K and an oxygen fugacity 2 log units below IW, we obtain $D_{Pt}^{met/sil} = 4.4(\pm 0.4) \times 10^8$ and $D_{Rh}^{met/sil} = 1.6(\pm 0.1) \times 10^6$. For comparison, the metal-silicate partition coefficient for Pd, $D_{Pd}^{met/sil}$, extrapolated to 3000°C using temperature-dependent data obtained at 1.5 GPa and log fO_2 = IW − 2, was estimated to be 8×10^3 by Holzheid et al. (2000). The Pd and Pt partitioning results of Holzheid et al. (2000) suggest that high pressure (at least up to 15 GPa) does not significantly affect the metal-silicate partition coefficients of these elements. It is therefore likely that the values of the Pt and Rh partition coefficients that we calculate here will not change much with pressure.

Calculated depletions of Pt and Rh in the Earth's mantle that would result from equilibrium core formation, based on the new solubility results, are shown in Figure 4. For comparison, the depletion values calculated using the Pt and Rh partition coefficients of Ertel et al. (1999), which were estimated without considering the effect of temperature, are also shown as well as the depletion value of Pd using the partition coefficient of Holzheid et al. (2000). The depletions of Pt and Rh calculated from our extrapolated partition coefficients, when compared to estimates of Ertel et al. (1999), reveal an important effect of temperature (>7 orders of magnitude). However, the calculated depletions of the elements are still lower than the observed mantle depletions by ~6 and 4 orders of magnitude for Pt and Rh, respectively. In addition, the calculated depletions for Pt, Rh, and Pd differ by orders of magnitude (~4 orders of magnitude difference between the depletions of Pt and Pd and ~2 orders of magnitude difference between those of Rh and Pd), which is inconsistent with the chondritic abundance ratio of the elements observed in the mantle (Lorand and Alard, 2000).

Note that in the above estimates of partition coefficients and mantle depletions of Pt and Rh, we have not taken into account the effect of silicate melt composition. Melt composition and the degree of polymerization of the melt (expressed as *NBO*/*T*) can have a large effect on the metal-silicate partition coefficients of siderophile elements. As observed by Walter and Thibault (1995), the metal-silicate melt partition coefficients of Mo and W decrease by ~2 orders of magnitude as the melt composition is changed from basaltic to peridotitic. In the case of Pt, experiments by Borisov and Palme (1997) showed that Pt solubility increases and its partition coefficient decreases only slightly with increasing *NBO*/*T* (increasing *NBO*/*T* from ~0.5 to ~1.3 leads to an increase in the solubility of Pt of only ~0.2 log units). Thus, the effect of composition alone appears to be insufficient to explain the difference between the observed depletion for Pt and the one predicted from our partitioning

data. Because it appears that high pressure cannot explain this difference either (Holzheid et al., 2000), our new results confirm that high-pressure and high-temperature core-mantle equilibrium during accretion of the Earth cannot result in the observed depletions of HSEs in the mantle. The abundances and relative chondritic ratios observed for these elements in the mantle remain better explain by the accretion of a late veneer of chondritic material after the core separated from the mantle. This conclusion is consistent with results of other recent studies (e.g., Holzheid et al., 2000).

6. CONCLUSIONS

Our solubility results confirm the highly siderophile nature of Rh and Pt, with solubilities at 1550°C, 1 bar, and log $fO_2 = -2.5$ being < 9 ppm for pure Rh and 1.5 ppm for pure Pt in silicate melt of anorthite-diopside eutectic composition. Although the solubilities of both elements in silicate melt increase with increasing temperature, values of partition coefficients for Pt obtained by extrapolation to likely core formation conditions still remain too high to explain the overabundances of these elements in the mantle (Fig. 4). Also, the metal-silicate partition coefficients for Pt and Rh differ by ~2 log units. During core formation involving core-mantle equilibrium, such a difference in partition coefficients would have differentiated Pt and Rh strongly so that these elements would not be observed in the Earth's mantle in a nearly chondritic ratio. Our results therefore support the addition of a late veneer of chondritic material to the Earth after core formation.

Acknowledgments—We are very grateful to Astrid Holzheid and two anonymous reviewers for their critical reviews of the manuscript, which helped greatly to improve its quality, and to Detlef Krausse for assistance with the electron microprobe. We also thank Fabrice Gaillard for his assistance with calculating the Pt activity coefficient. This work was partially supported by the EU TMR Large Scale Facility program and partially funded by Deutsche Forschungsgemeinschaft grants to D. B. Dingwell (DFG Di 431).

Associate editor: B. Mysen

REFERENCES

Barin I. (1989) Platinum. In: *Thermochemical Data of Pure Substances—Part II* (ed. I. Barin), pp. 1184–1185. Cambridge University Press, New York.

Borisov A. and Palme H. (1997) Experimental determination of the solubility of platinum in silicate melts. *Geochim. Cosmochim. Acta* **61,** 4349–4357.

Borisov A. and Palme H. (1998) Experimental determination of osmium metal-silicate partitioning coefficient. *N. Jb. Miner. Abh.* **172,** 347–356.

Borisov A., Palme H., and Spettel B. (1994) Solubility of Palladium in silicate melts: Implications for core formation in the Earth. *Geochim. Cosmochim. Acta* **58,** 705–716.

Dingwell D. B., O'Neill H. S., Ertel W., and Spettel B. (1994) The solubility and oxidation state of nickel in silicate melt at low oxygen fugacities: Results using a mechanically assisted equilibration technique. *Geochim. Cosmochim. Acta* **58,** 1967–1974.

Ertel W., Dingwell D. B., and O'Neill H. S. (1996) Solubility of tungsten in a haplobasaltic melt as a function of temperature and oxygen fugacity. *Geochim. Cosmochim. Acta* **60,** 1171–1180.

Ertel W., O'Neill H. S., Sylvester P. J., and Dingwell D. B. (1999) Solubilities of Pt and Rh in a haplobasaltic silicate melt at 1300°C. *Geochim. Cosmochim. Acta* **63,** 2439–2449.

Ertel W., O'Neill H. S., Sylvester P. J., Dingwell D. B., and Spettel B. (2001) The solubility of rhenium in silicate melts: Implications for the geochemical properties of rhenium at high temperature. *Geochim. Cosmochim. Acta* **65,** 2161–2170.

Günther D., Frischknecht R., and Heinrich C. A. (1997) Capabilities of a 193 nm ArF excimer laser for LA-ICP-MS microanalysis of geological materials. *J. Anal. At. Spectrom.* **12,** 939–944.

Holzheid A., Sylvester P. J., O'Neill H. S., Rubie D. C., and Palme H. (2000) Evidence for a late veneer in the Earth's mantle from high pressure partitioning of palladium and platinum. *Nature* **406,** 396–399.

Hultgren R., Desai P. D., Hawkins D. T., Gleisen M., and Kelley K. K. (1971) Fe-Pt binary alloy. In: *Selected Values of the Thermodynamic Properties of Binary Alloys—Part 2*, pp. 861–865. American Society for Metals, Materials Park, OH.

Jacob K. T., Priya S., and Waseda Y. (1998) Thermodynamic properties and phase equilibria for Pt-Rh alloys. *Metall. Mater. Trans. A* **29,** 1545–1550.

Jones J. H. and Drake M. J. (1986) Geochemical constraints on core formation in the Earth. *Nature* **322,** 221–228.

Kimura K., Lewis R. S., and Anders E. (1974) Distribution of gold and Rhenium between nickel-iron and silicate melt: Implication for the abundance of siderophile elements on the Earth and Moon. *Geochim. Cosmochim. Acta* **38,** 683–701.

Li J. and Agee C. B. (1996) Geochemistry of mantle-core formation at high pressure. *Nature* **381,** 686–689.

Longerich H. P., Jackson S. E., and Günther D. (1996) Laser ablation inductively coupled plasma mass spectrometry transient signal data acquisition and analyte concentration calculation. *J. Anal. At. Spectrom.* **11,** 899–904.

Lorand J. P. and Alard O. (2000) Platinum-group element abundances in the upper mantle: New constraints from in situ and whole-rock analyses of Massif Central xenoliths (France). *Geochim. Cosmochim. Acta* **65,** 2789–2806.

McDonough W. F. and Sun S.-S. (1995) The composition of the Earth. *Chem. Geol.* **120,** 223–253.

Mukhopadahyay B., Basu S., and Holdaway M. (1993) A discussion of Margules-type formulations for multicomponent solutions with a generalized approach. *Geochim. Cosmochim. Acta* **57,** 277–283.

Murthy V. R. and Karato S. (1997) Core formation and chemical equilibrium in the earth—II: Chemical consequences for the mantle and core. *Phys. Earth Planet. Int.* **100,** 81–95.

Nafziger R. H., Ulmer G. C., and Woermann E. (1971) Gaseous buffering at one atmosphere. In: *Research Techniques for High Pressure and High Temperature* (ed. G. C. Ulmer). Springer-Verlag, Berlin, Germany.

O'Neill H. S. (1991) The origin of the moon and the early history of the Earth: A chemical model. Part 2, the Earth. *Geochim. Cosmochim. Acta* **55,** 1159–1172.

O'Neill H. S. and Pownceby M. I. (1993) Thermodynamic data from redox reactions at high temperatures. I. An experimental and theoritical assessment of the electrochemical method using stabilized zirconia electrolytes with revised values for Fe-"FeO," Co-CoO, Ni-NiO and Cu-Cu_2O oxygen buffers, and new data for the W-WO_2 buffer. *Contrib. Miner. Petrol.* **114,** 296–314.

Righter K. and Drake M. J. (1997) Metal-silicate equilibrium in a homogeneously accreting earth: New results for Re. *Earth Planet. Sci. Lett.* **146,** 541–553.

Righter K., Drake M. J., and Yaxley G. (1997) Prediction of siderophile element metal/silicate partition coefficients to 20 GPa and 2800°C: The effect of temperature, pressure, oxygen fugacity and silicate and metallic melt compositions. *Phys. Earth Planet. Int.* **100,** 115–134.

Swartzendruber L. J. (1984) The Fe-Rh (iron-rhodium) system. *Bull. Alloy Phase Diagrams* **5,** 456–462.

Sylvester P. J. and Eggins S. M. (1997) Analysis of Re, Au, Pd, Pt and Rh in NIST glass certified reference materials and natural basalt glasses by laser ablation-ICP-MS. *Geostan. News.* **21**(2), 215–229.

Walker D. (2000) Core participation in mantle geochemistry: Geochemical Society Ingerson Lecture, GSA Denver, October 1999. *Geochim. Cosmochim. Acta* **64,** 2897–2911.

Walter M. J. and Thibault Y. (1995) Partitioning of tungsten and molybdenum between metallic liquid and silicate melt. *Science* **270,** 1186–1189.